In-Line Fiber-Optic Near-Infrared Spectroscopy: Monitoring of Rheological Properties in an Extrusion Process. Part II.

S. VEDULA, M. G. HANSEN

Department of Chemical Engineering, 419 Dougherty Building, University of Tennessee, Knoxville, Tennessee 37996–2200

Received 14 November 1996; accepted 8 July 1997

ABSTRACT: In an extrusion process, linear viscoelastic properties of molten poly(ethylene vinyl acetate) (EVA) copolymers, which have one principal factor of variation, can be estimated from in-line near-infrared (NIR) spectra. The NIR transmission spectra of molten polymer flow stream were collected in a flow cell attached to a single-screw extruder. Dynamic rheological functions obtained from linear viscoelastic measurements, for example, the complex viscosity response, are regressed against the NIR spectra. The primary method for the rheological measurements involved sinusoidal, oscillatory shear experiments at varying angular frequencies using a cone-and-plate viscometer. All measurements were carried out on molten EVA polymers at 200°C. Calibration models were built on spectra in the carbon—hydrogen (C—H) vibrational stretch, first overtone, wavelength region (1620–1840 nm), and these models were used to predict the rheological material functions of copolymer samples. The robustness of these models was tested on independent prediction samples that had not been included in the calibration models. © 1998 John Wiley & Sons, Inc. J Appl Polym Sci 68: 873–889, 1998

Key words: in-line; complex viscosity; near-infrared spectroscopy; extrusion; copolymer

INTRODUCTION

The objective of this study is to extend the applicability of NIR spectroscopy in making direct, simultaneous measurements of physical properties and chemical composition in process real time. In a previous publication, a methodology was detailed for correlating the polymer melt flow index (MI) with NIR absorption spectra.[1] In this work, simultaneous predictions were made of comonomer composition and MI of flowing, molten EVA copolymers during extrusion, using NIR spectra in the C—H stretch first overtone region (1620–1840 nm). A procedure using multivariate statistical techniques was detailed to separate two independent factors of variation in the NIR absorption spectra, namely the primary, dominant effects of comonomer composition and the secondary rheological effects due to anisotropic flow behavior in the optical measurement volume. Separate calibration and validation models were developed for predicting vinyl acetate (VA) concentration and MI, on samples belonging to two different groups. One group consisted of EVA samples with similar VA content and varying MI. The second group consisted of samples with varying VA content but similar MI values. The ability of the models to independently predict VA content as well as MI for the two different sample groups reiterated the fact that MI is not related to chemical composition, but there was sufficient information in the NIR absorption spectra to estimate polymer MI.

Correspondence to: M. G. Hansen.

Journal of Applied Polymer Science, Vol. 68, 873–889 (1998)
 CCC 0021-8995/98/060873-17

The following work describes a methodology to estimate such rheological properties as dynamic linear viscoelastic material functions from the NIR spectra of EVA copolymers. The linear viscoelastic properties of interest for the current study are complex viscosity $|\eta^*(\omega)|$ responses (ω, the angular frequency) of EVA copolymers, which are obtained from sinusoidal, oscillatory, shear experiments. In addition to quantitative calibration models, this study will focus on theoretical considerations for the origin of rheological response in the NIR spectra. Qualitative results from multivariate analysis will be detailed, and the models will be tested in a real-time extrusion process.

EXPERIMENTAL

For this study, EVA copolymers from two independent sources were utilized for the linear viscoelastic experiments. These sample sets will be referred to, henceforth, as Group I and Group II samples. Group I is comprised of 14 samples of EVA copolymers from one manufacturer, and Group II is comprised of five EVA samples from a second manufacturer. The existence of two separate sets of polymer samples provided the advantage of preparing calibration models on one set of polymer samples and using the second set as an independent test set to validate the precision of the calibration models. This would also test the ability of the calibration models to predict the desired properties in light of external variations, such as processing differences during polymerization, etc.

The linear viscoelastic measurements were performed on molten EVA samples at 200°C with a Rheometrics™ Dynamic Stress Rheometer. The samples were compression molded into disks, 25 mm in diameter, which were melted in the rheometer at the desired temperature. A 25-mm diameter cone-and-plate viscometer with a gap angle of 0.1 radians (rad) was used for these measurements. Constant amplitude, sinusoidal, shear stress at 200 Pa was applied to the molten sample, and rheological measurements were made over a wide range of angular frequencies, ω, from 0.01 to 500 rad/s. At a stress of 200 Pa, the EVA samples exhibited rheological responses in the linear viscoelastic region over several decades of frequency. The properties of interest were measured at 12 frequency values per decade. A continuous purge of dry nitrogen gas prevented any sample degradation, or moisture absorption, from the ambient atmosphere. The properties obtained from these experiments are the storage modulus $G'(\omega)$, loss modulus $G''(\omega)$, and $|\eta^*(\omega)|$ as a function of ω. Figure 1 illustrates a typical plot of the linear viscoelastic response for an EVA sample with 9.08 wt % VA concentration and $\bar{M}_w$ of 228,000.

Large experimental scatter was observed in the $G'(\omega)$ measurements for samples with low $\bar{M}_w$ (low melt viscosity or high MI values) at small ω values ($\omega < 0.3$ rad/s). This was attributed to limitations in instrument accuracy for measurements of low $G'(\omega)$ values [$G'(\omega) < 0.0001$ Pa]. Similarly, sample losses were observed at higher frequencies ($\omega > 150$ rad/s), and the actual applied shear stress differed from the control stress. This led to some noise in the measurements. Therefore, only data in the frequency range, $\omega = 0.38$ rad/s to $\omega = 122$ rad/s, were considered for analysis. Figure 2 shows an overlaid plot of the complex viscosity, $|\eta^*(\omega)|$, response, with varying ω, for the EVA samples. These measurements were used as the reference values for the data analysis.

The experimental setup and details for collecting the NIR absorption spectra were outlined in the previous publication.[1]

DATA ANALYSIS

Compared to MI calibration, quantitative analysis for complex viscosity response from NIR absorption spectra is more complex, and mathematical modeling involves a combination of several multivariate techniques, such as principal component analysis (PCA)[2] and partial least squares (PLS).[3,4] A schematic representation for correlating the $|\eta^*(\omega)|$ response to NIR absorption spectra is shown in Figure 3. There is one major difference in this analysis as compared with the MI calibration discussed before. The property being calibrated, $\mathbf{Y}$ ($|\eta^*(\omega)|$ response), can no longer be represented as a vector, or an $m \times 1$ matrix (calibration of MI or VA concentration). The $|\eta^*(\omega)|$ values at varying ω for the EVA samples are put in a matrix with several columns, or variables. Each column in this matrix represents the $|\eta^*(\omega)|$ values at a single ω value. Therefore, the number of columns, n, in the matrix equals the total number of frequencies at which the linear viscoelastic properties were measured. The rows in the matrix correspond to the rheological response for different samples used in the calibration. If m samples are used for calibration, then

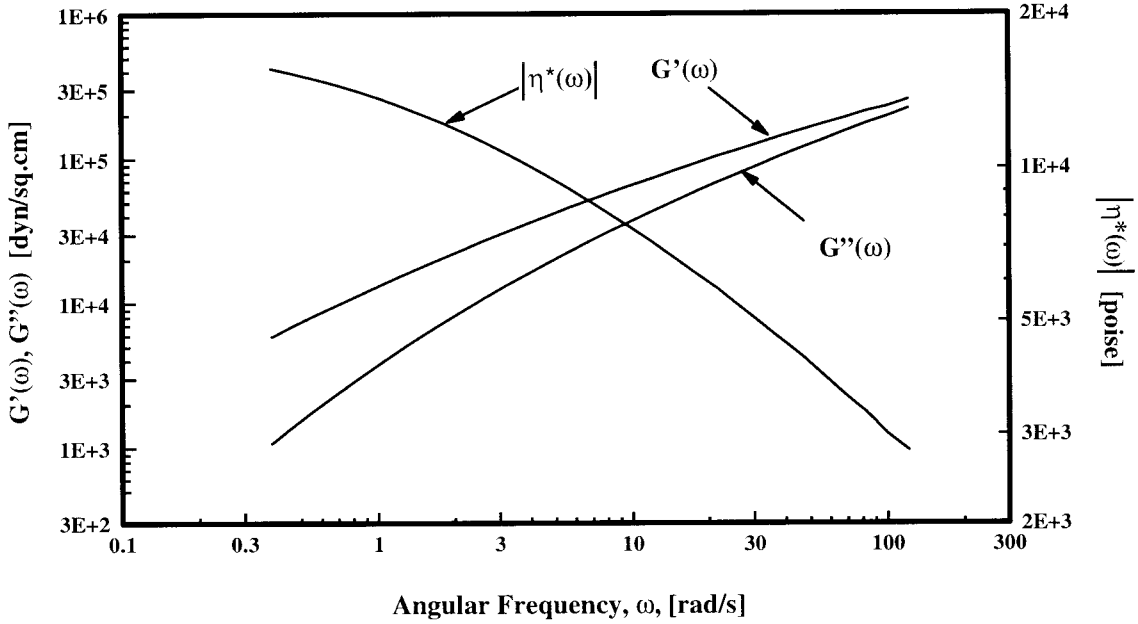

Figure 1 Plot of the dynamic rheological properties versus angular frequency for an EVA sample with 9.08 wt % VA content and $\bar{M}_w$ of 228,000. The measurements were carried out under a shear stress of 200 Pa and at isothermal conditions of 200°C.

Y is of size $m \times n$. Similarly, in the **X** matrix ($m \times k$), the rows correspond to the absorbance values for different samples, and the columns correspond to absorbance values at different wavelengths (a total of k wavelengths).

A variety of regression techniques can be used to develop calibration models for data with multiple columns of **Y**. The first methodology, PLS-1, treats each column in **Y** as a single variable that would be independently regressed against the ab-

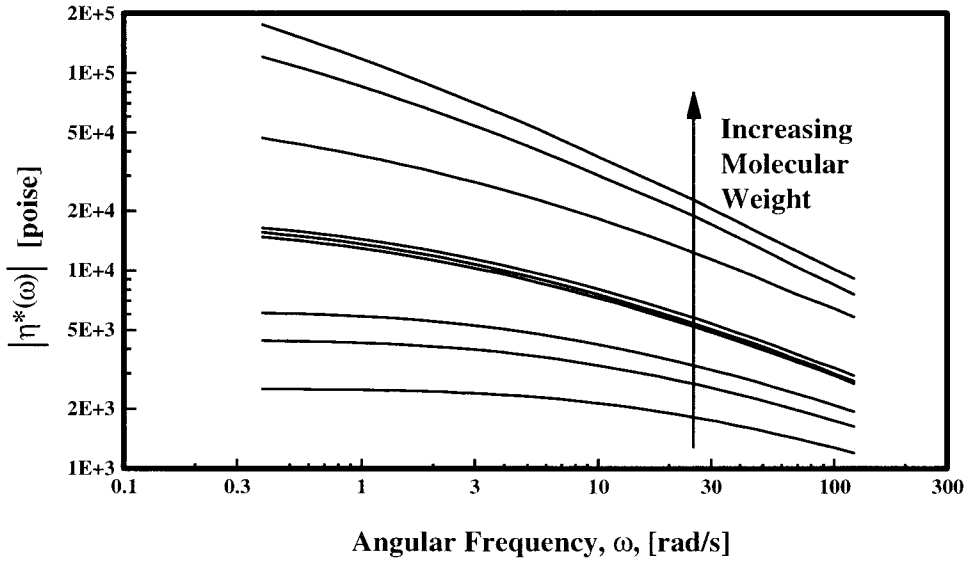

Figure 2 Overlaid plot of the complex viscosity response for EVA samples over an angular frequency range of 0.38 rad/s to 122 rad/s. The measurements were carried out under a shear stress of 200 Pa and at 200°C.

$$\mathbf{Y}^{(m \times n)} = \mathbf{X}^{(m \times p)} \cdot \alpha^{(p \times n)}$$

$$\begin{bmatrix} \log(\eta^*(\omega_1, MI_1)) & \log(\eta^*(\omega_2, MI_1)) & \cdots & \log(\eta^*(\omega_n, MI_1)) \\ \log(\eta^*(\omega_1, MI_2)) & \log(\eta^*(\omega_2, MI_2)) & \cdots & \log(\eta^*(\omega_n, MI_2)) \\ \vdots & \vdots & & \vdots \\ \log(\eta^*(\omega_1, MI_m)) & \log(\eta^*(\omega_2, MI_m)) & \cdots & \log(\eta^*(\omega_n, MI_m)) \end{bmatrix} = \begin{bmatrix} \text{NIR spectra} \end{bmatrix} \begin{bmatrix} \alpha_{11} & \alpha_{12} & \cdots & \alpha_{1n} \\ \alpha_{21} & \alpha_{22} & \cdots & \alpha_{2n} \\ \vdots & \vdots & & \vdots \\ \alpha_{p1} & \alpha_{p2} & \cdots & \alpha_{pn} \end{bmatrix}$$

Figure 3 Schematic representation for correlation of $|\eta^*(\omega)|$ with NIR absorbance spectra. The complex viscosity response in the **Y** matrix is regressed against the NIR spectral data (**X** matrix), using multivariate statistical analysis.

sorbance matrix.[4] Thus, n calibration models are developed (for n variables in **Y**), one for the $|\eta^*(\omega)|$ vector at each ω. In each of these n models, the principal components are evaluated by maximizing the covariance of $\mathbf{X}^T\mathbf{y}_j$, where $\mathbf{y}_j$ is the j-th column of matrix **Y**. However, these calculations can be done only at the expense of valuable computational time. Also, the use of PLS-1 provides little information about the relationship between response variables in the **Y** matrix.

Another technique, entitled PLS-2 regression, treats all response variables as a single variable or block, and regression is performed on the **Y** matrix as a whole.[4] Thus, PLS-2 involves building a single calibration model for the entire **Y** matrix. An important observation is made regarding the use of PLS-2 on several response variables while evaluating the optimal number of factors. If the response variables in the **Y** matrix are independent of each other, or are not intercorrelated, then the number of factors required for building optimal models would be different for each response variable. However, PLS-2 gives only one such value for the number of factors, and this leads to a calibration model that overfits some variables and underfits others. However, if the response variables are highly intercorrelated, PLS-2 calibration is a good choice for analysis. Again, developing a calibration model using PLS-2 requires extensive computations, as it requires evaluating the SVD of a large covariance matrix.

To circumvent these problems, a more efficient methodology based on an earlier study is used for the current work.[5] This methodology involves initial identification of the principal factors of variation, or the principal components, in the **Y** matrix alone. These principal components often relate to the actual, physical factors of variation in the data. For example, it is known that the linear viscoelastic response (**Y** matrix) of the EVA samples is governed by the $\bar{M}_w$ and MWD parameters. Therefore, the differences in $|\eta^*(\omega)|$ values, which form the **Y** matrix, can be attributed to varying $\bar{M}_w$ and MWD values in these samples. If the response variables forming the **Y** matrix are highly intercorrelated (this would happen if there were only a small number of independent physical factors affecting the data), then the matrix can be decomposed into a small number of principal components that explain most of the variance in **Y**. In the above example, if the only difference in the complex viscosity response of all EVA samples were due to variation in only one physical parameter, say $\bar{M}_w$ values, then only one principal component will sufficiently explain most of the **Y**-data variance.

The linear viscoelastic behavior of these copolymers is typical of a class of polymers that are thermo-rheologically simple.[6,7] For such polymers, the rheological behavior is oversimplified, due to the absence of factors, such as phase separation, and the viscoelastic response is influenced primarily by structural variations, which are governed by molecular weight parameters. Therefore, for such polymers, it is expected that only a few factors will sufficiently explain most of **Y**-data

variance. This methodology of identifying the main factors of variation using multivariate analysis can potentially serve as a mathematical approach to separate contributions from different parameters that affect the rheological behavior.

Decomposition of the **Y** matrix into principal components can be carried out by PCA analysis. Using SVD, PCA is performed on the **Y**-data to yield the following result:

$$\mathbf{Y} = \mathbf{U_{PCA}}\,\Sigma_{\mathbf{PCA}}\,\mathbf{V_{PCA}^{T}} \quad (1)$$

where the columns of $\mathbf{U_{PCA}}$ are the eigenvectors of $\mathbf{YY}^{T}$, the columns of $\mathbf{V_{PCA}}$ are the eigenvectors of $\mathbf{Y}^{T}\mathbf{Y}$, and $\mathbf{\Sigma_{PCA}}$ is a diagonal matrix containing the eigenvalues. $\mathbf{V_{PCA}^{T}}$ is the transpose matrix of $\mathbf{V_{PCA}}$. The subscript **PCA** is used to identify results obtained from PCA analysis (Later on, such decomposition will be carried out for PLS as well). The first k principal components are defined as:

$$\mathbf{T_{PCA}} = [\mathbf{t_{1,PCA}}, \ldots, \mathbf{t_{k,PCA}}] = [\sigma_{1,\mathrm{PCA}}\mathbf{U_{1,PCA}}, \ldots, \sigma_{k,\mathrm{PCA}}\mathbf{U_{k,PCA}}] \quad (2)$$

PCA decomposition is performed, such that the principal components, or latent variables, or eigenvectors are evaluated in the order of their relative importance in explaining the data variance. Thus, the first few factors explain maximum "information" in the data, and the latter factors contain only random noise. Using this criterion, the first k significant principal components are selected.

In the next step, the smaller matrix $\mathbf{T_{PCA}}$ ($m \times k$) is used for PLS regression against the NIR absorbance matrix, **X**. The regression equation for the vectors, $\mathbf{t_{j,PCA}}$ (j-th column of $\mathbf{T_{PCA}}$), is expressed as follows:

$$\hat{\mathbf{t}}_{\mathbf{j,NIR}} = \mathbf{X}\beta_j \quad (3)$$

where $\hat{\mathbf{t}}_{\mathbf{j,NIR}}$ ($m \times 1$) is the NIR predicted value of $\mathbf{t_{j,PCA}}$ ($m \times 1$) obtained from PLS regression. β_j ($n \times 1$) is a vector containing the regression coefficients. After regression of vectors $\mathbf{t_{j,PCA}}$, the original variables in the **Y** matrix are regenerated by estimating the regression coefficients, α, from the following relationship:

$$\hat{\mathbf{Y}} = \mathbf{X}\alpha \quad (4)$$

The new set of regression coefficients, α, are related to $\mathbf{B} = [\beta_1, \ldots, \beta_k$ by the following expression:

$$\alpha = [\beta_{\mathbf{1}}, \ldots, \beta_{\mathbf{k}}][\mathbf{V_{1,PCA}}, \ldots, \mathbf{V_{k,PCA}}]^{T} \quad (5)$$

An alternate and equivalent expression that relates the predictions for **Y** with predicted $\mathbf{t_{j,NIR}}$, $\{j = 1, \ldots, k\}$ is written as follows:

$$\hat{\mathbf{Y}} = [\hat{\mathbf{t}}_{\mathbf{1,NIR}}, \ldots, \hat{\mathbf{t}}_{\mathbf{k,NIR}}][\mathbf{V_{1,PCA}}, \ldots, \mathbf{V_{k,PCA}}]^{T} \quad (6)$$

For the complex viscosity calibration, data will be presented in the following section that will support the conclusion that there is only one significant factor of variation in **Y**. Thus, from PCA analysis, it will be shown that $k = 1$, and the PLS-1 regression model will be built only for the first factor.

Scores and Loadings

In this section, scores and loadings matrices are introduced as tools that aid in the qualitative interpretation of multivariate analysis. By definition, each principal component is associated with a "score" and a "loading" vector. (A principal component is obtained by the product of the corresponding score and loading vector.) The loading vectors constitute the columns of matrix **V**, which is obtained by decomposition. These vectors display the clustering of the independent variables (e.g., ω) into classes that are used in explaining the variance in the data. Thus, the loading values can be viewed as "weights" associated with each independent variable, and they describe the relative importance of the independent variables in regression. The score vectors are made up of the columns of matrix **T**, and their values are "magnitudes" that are multiplied by the corresponding loading vectors. The score values characterize the relationship between the samples. For example, a linear score vector would imply a linear relationship between the samples. More information about these matrices and their interpretation can be found in Refs. 2–4. In the following sections, these matrices will be used to provide useful information about the regression.

RESULTS AND DISCUSSION

This section discusses the results obtained for the prediction of $|\eta^*(\omega)|$ response from in-line NIR absorption spectra. The linear viscoelastic experi-

Table I PCA on the Y Matrix Containing the Complex Viscosity Values: Contribution from Each Principal Component

Principal Component Number	Variance Explained by This Factor (%)	Overall Variance Explained (%)
1	99.82	99.82
2	0.17	99.99
3	0.01	100.00

ments in the angular frequency range of $\omega = 0.38$ rad/s to $\omega = 122$ rad/s were used for building the **Y** matrix. The $|\eta^*(\omega)|$ values were measured at a total of 31 discrete ω-values in this range. In a similar manner to MI calibration, the natural logarithms of the complex viscosity response were included in the analysis.[1] Thus, the **Y** matrix is composed of $\ln(|\eta^*(\omega)|)$ values.

Ten samples, nine from Group I and one from Group II, were included in the calibration set. The Group II sample was required in the calibration because one sample in Group II had VA concentration outside the range of Group I sample concentrations. The model developed on samples in the calibration set was used to predict samples in an independent prediction set. Four samples from Group I and four samples from Group II were used in the prediction set. For the calibration, ten replicate NIR spectra were collected in-line for all the samples. One spectrum, the average of these replicate spectra for each sample, was used to construct the calibration set. As for MI calibration, absorbance spectra in the wavelength range of 1620–1840 nm were used for regression. First derivatives of the absorbance spectra were utilized for calibration, in order to remove baseline offsets.

PCA of Y Matrix: Decomposition into Principal Components

The **Y** matrix of $\ln(|\eta^*(\omega)|)$ values was standardized by mean-centering. Prior to PLS regression for obtaining the regression coefficients, PCA was performed on the **Y** matrix to decompose it into a smaller matrix, $\mathbf{T_{PCA}}$. This matrix is made up of the first few principal components that are required to quantify most of the information in $\ln(|\eta^*(\omega)|)$ data. As shown in Table I, only one principal component was sufficient to explain 99.8% of the variance in the $\ln(|\eta^*(\omega)|)$ data.

This result implies that, in the set of EVA samples used for this study, there is only physical factor responsible for variation in rheological response (which is due to change in $\bar{M}_w$ values). With increasing $\bar{M}_w$ values, a positive shift is observed in the complex viscosity curves. A qualitative interpretation of the first principal component is brought about from the loading ($\mathbf{V_{1,PCA}}$) and the score ($\mathbf{t_{1,PCA}}$) vector obtained from PCA decomposition. In Figure 4, the first loading vector is plotted against the angular frequency, ω. As expected, the first loading vector is representative of an "average" complex viscosity curve, which explains the general trend in variation of the complex viscosity response for different ω values. In such a case, the score vector is made of magnitudes or vertical shift factors, which when multiplied with the average loading spectrum, gives the individual complex viscosity curve for each sample. Similar horizontal shifting procedures are commonly used by rheologists to generate master curves to account for variations in temperature and molecular weight.[6] As an example, such shift factors are utilized to relate the specific viscosity to concentration in polymer solutions by scaling the molecular weight dependence. The above procedure can be viewed as an alternate mathematical approach to achieve similar shifting effects through eigenvector rotation, instead of commonly used superposition principles, which use curve-fitting strategies to obtain the shift factors. A comparison between the two methodologies shows that the loading vector is analogous to a master curve, while the score vector includes shift factors for individual curves. However, the current method using multivariate analysis, does not increase the range of ω values unlike the normal superposition procedures.[6]

In the rheology data, if there were other additional effects, or factors of variation, the variance in the complex viscosity functions could not be represented by a single shift. In such cases, additional principal components would be required to account for these parametric effects. In other words, more than one principal component would be required to explain significant variance in **Y**.

From the above analysis, it is seen that the **Y** matrix can be reduced into a single vector $\mathbf{t_{1,PCA}}$, which corresponds to the eigenvector associated with the largest eigenvalue. The original **Y** matrix is regenerated from the decomposed principal components using eq. (6), which can be rewritten as follows:

$$\mathbf{Y_{reg}} = \mathbf{t_{1,PCA}}\mathbf{V_{1,PCA}^T} \quad (7)$$

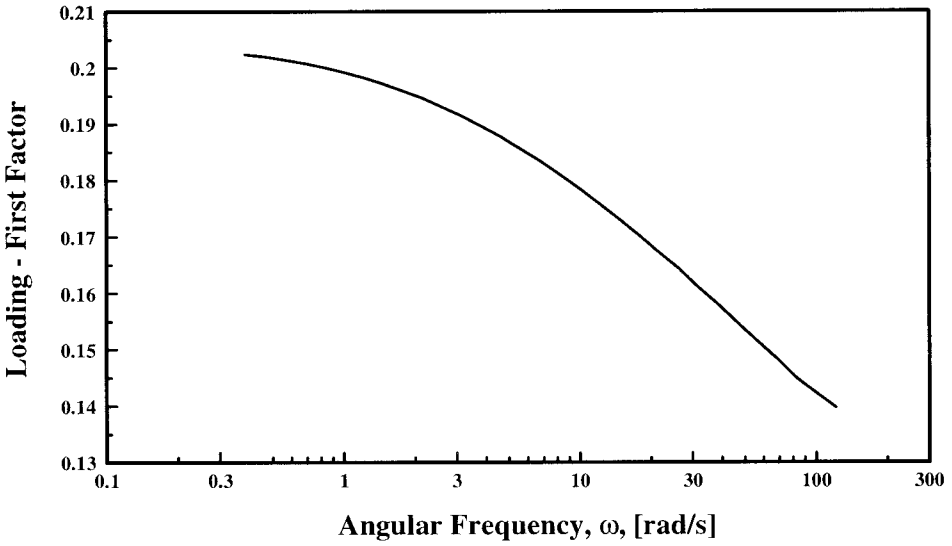

Figure 4 PCA analysis of **Y** matrix containing the complex viscosity data: Plot of loading vector for the first principal component represents the average complex viscosity curve. The magnitudes or "vertical shift factors" in the first score vector are multiplied with the loading curve to produce the original complex viscosity curves.

where $\mathbf{Y}_{\mathbf{reg}}$ is the regenerated **Y** matrix, $\mathbf{t}_{\mathbf{1,PCA}}$ is the first column of $\mathbf{T}_{\mathbf{PCA}}$ and $\mathbf{V}_{\mathbf{1,PCA}}$ is the first column of $\mathbf{V}_{\mathbf{PCA}}$. Equation (7) provides a framework for comparing the original response variables, $\ln(|\eta^*(\omega)|)$ values in the **Y** matrix, to the regenerated matrix, $\ln(|\eta^*(\omega)|)$ values in $\mathbf{Y}_{\mathrm{reg}}$. It shows how well the information in the **Y** matrix can be obtained by using only one principal com-

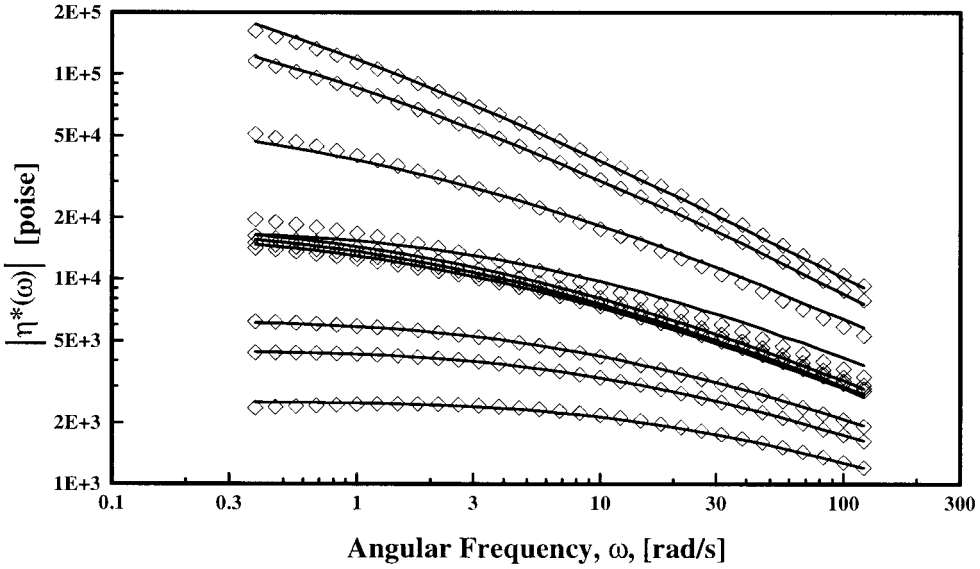

Figure 5 PCA analysis of **Y** matrix containing complex viscosity response: Plot comparing the original **Y** matrix (symbol—solid line) with the regenerated matrix, $\mathbf{Y}_{\mathbf{reg}}$, (symbol— ◇) which is obtained from one principal component PCA model. The excellent fit between the two curves shows that one factor is sufficient to represent significant variance in **Y** matrix.

Table II PLS Regression on the Reduced Matrix: Contribution from Each Principal Component

Principal Component Number	$\mathbf{t}_{1,PCA}$ Calibration Model: Overall Explained Variance in $\mathbf{t}_{1,PCA}$ (%)
1	31.5
2	94.9
3	98.2
4	99.6

ponent. Figure 5 illustrates this feature; the complex viscosity responses, $|\eta^*(\omega)|$, from $\mathbf{Y}$ and $\mathbf{Y}_{reg}$ are plotted against ω.

PLS-1 Regression of the Reduced Matrix, $\mathbf{t}_{1,PCA}$: Regression onto X

After PCA, a PLS-1 regression model is developed for correlating $\mathbf{t}_{1,PCA}$, of size $(m \times 1)$, onto the NIR absorbance matrix, $\mathbf{X}$. In this section, the PLS results are discussed in detail. The PLS calibration is developed on the first derivatives of the absorbance spectra, using the leave-a-sample (LAS) crossvalidation technique, as discussed earlier.[1] Based on the PRESS criterion coupled with an *F*-statistic criterion, a four-principal component model was chosen for calibration. In Table II, the contribution of each principal component is listed, in explaining the variance in the reduced matrix $\mathbf{t}_{1,PCA}$. It is observed that 99.6% of the variance in $\mathbf{t}_{1,PCA}$ can be explained by four factors. Once the optimal number of factors to be included in the calibration model is decided, a final calibration model is developed from all samples in the calibration set. This model is used to predict the desired properties of samples from an independent prediction set.

Figure 6 shows the in-line NIR predicted $\hat{\mathbf{t}}_{1,NIR}$ for samples in the calibration and prediction sets, with a calibration model based on four factors. The deviations of the NIR predicted $\hat{\mathbf{t}}_{j,NIR}$ values from actual $\mathbf{t}_{1,PCA}$ values are expressed as residual errors for both the calibration and the prediction sets. These residual errors dictate the prediction capability of the calibration model. The SEC value, or the standard residual error for calibration, was 0.38, and the SEP value, the standard residual error for samples in the prediction set, was 0.80. When the entire complex viscosity response, $\hat{\mathbf{Y}}$, for the samples is regenerated using the predicted $\hat{\mathbf{t}}_{j,NIR}$ values [this can be done by replacing $\mathbf{t}_{1,PCA}$ with $\hat{\mathbf{t}}_{j,NIR}$ in eq. (7)], these residual errors translate into prediction errors for $|\eta^*(\omega)|$ values at each ω. The regenerated $|\eta^*(\omega)|$ response curves for samples in the calibration set are shown in Figure 7. Similarly, the predicted $|\eta^*(\omega)|$ response curves for samples in the prediction set are compared with the laboratory measured response curves in Figure 8. In these figures, the deviations of the in-line NIR predicted curves from the laboratory-measured

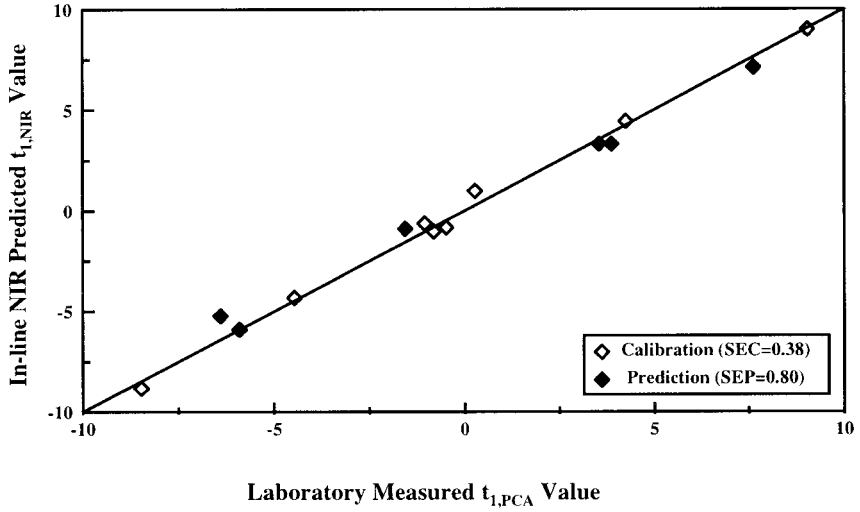

Figure 6 PLS calibration of $\mathbf{t}_{1,PCA}$ with regression against NIR absorbance data: predictions of $\hat{\mathbf{t}}_{1,NIR}$ for samples in the calibration and prediction sets. The standard errors associated with the calibration and prediction sets are SEC = 0.38 and SEP = 0.80, respectively.

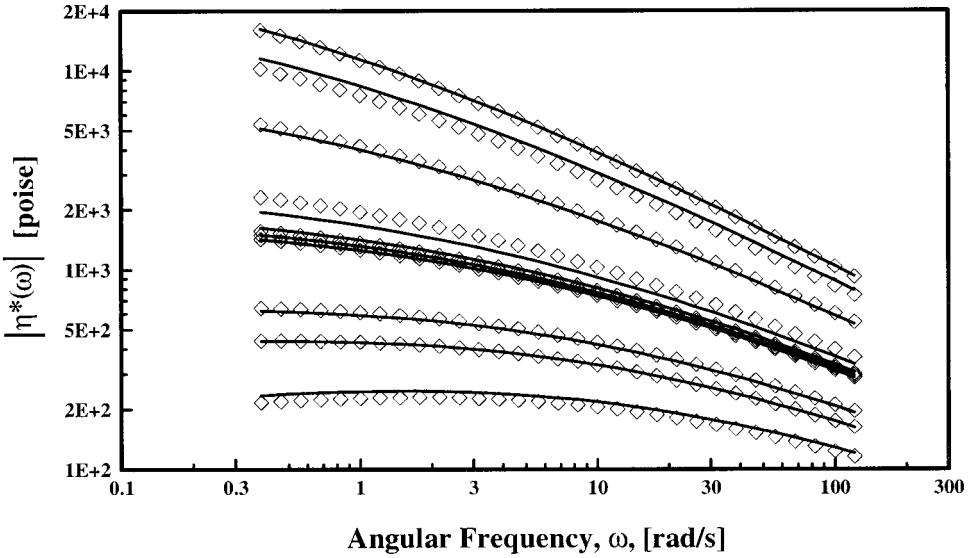

Figure 7 Calibration set: predictions for rheological response— $|\eta^*(\omega)|$ versus ω— for EVA samples. The complex viscosity curves are regenerated from the PLS-predicted $\hat{\mathbf{t}}_{1,\mathrm{NIR}}$ values using eq. (7). The standard error associated with the calibration set is SEC = 0.38. The solid curve represents the original curve, and the symbol ◇ represents the PLS-predicted curve.

response curves in the calibration and prediction sets correspond to the residual errors in the calibration model.

In a similar manner to PCA, PLS analysis also results in score and loading matrices.[2–4] A plot of the loading vector for the first principal component against NIR wavelengths, shown in Figure 9, typically resembles the average derivative spectrum.[1] The first principal component is expected to contain information about VA content, which

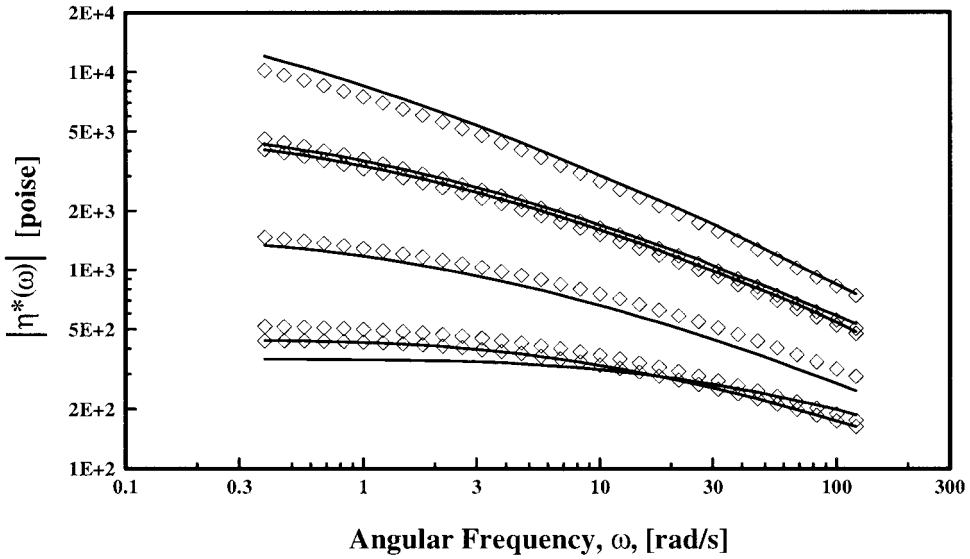

Figure 8 Prediction set: predictions for rheological response— $|\eta^*(\omega)|$ versus ω— for EVA samples. The complex viscosity curves are regenerated from the PLS-predicted $\hat{\mathbf{t}}_{1,\mathrm{NIR}}$ values using eq. (7). The standard error associated with the prediction set is SEP = 0.80. The solid curve represents the original curve, and the symbol ◇ represents the PLS-predicted curve.

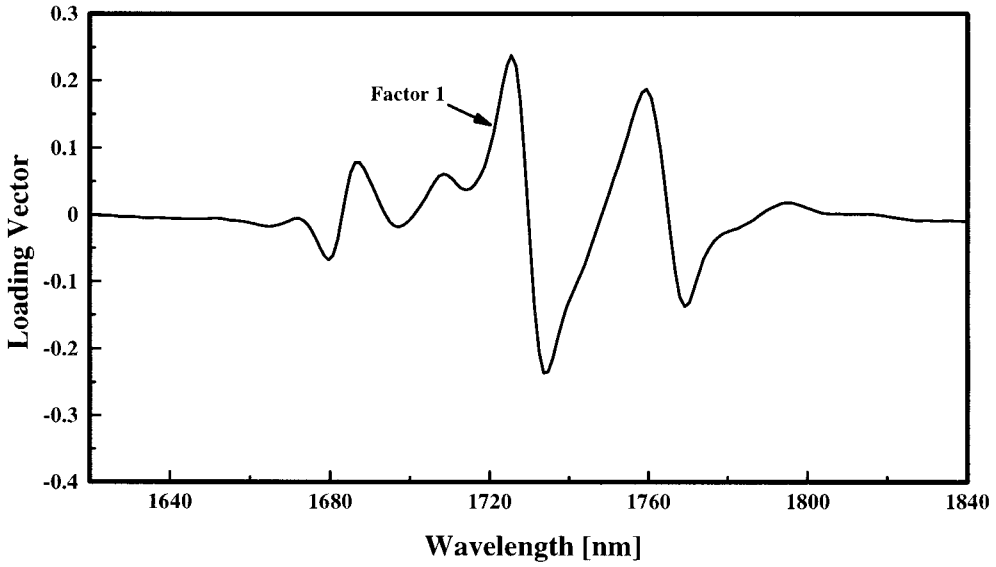

Figure 9 PLS calibration of $\mathbf{T}_{1,PCA}$: loadings plot for the first factor. The loading vector for the first principal component contains information about VA content (primary variation) in the EVA copolymers. The loading weights are higher in the wavelength region corresponding to the C—H stretch peaks.

is the dominant variable. For regression, wavelengths with larger loading values are relatively more important (in explaining variance in the response variables) than wavelengths with lower loading values. From the first loading plot, it is observed that information for VA content lies in the wavelength range of 1720–1780 nm, which contains the polyethylene doublet peaks in the original absorbance spectra.[1] The score vector for the first principal component is plotted against the VA concentration, as shown in Figure 10, which shows a linear trend, as expected. There-

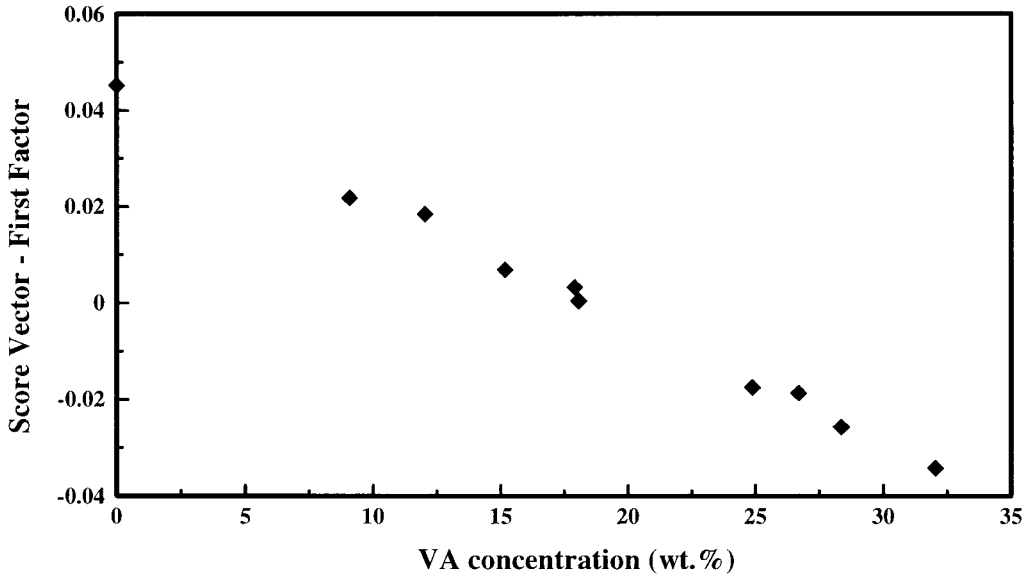

Figure 10 PLS calibration of $\mathbf{t}_{1,PCA}$: scores plot for the first factor. The score vector for the first principal component shows a linear trend with varying VA concentration.

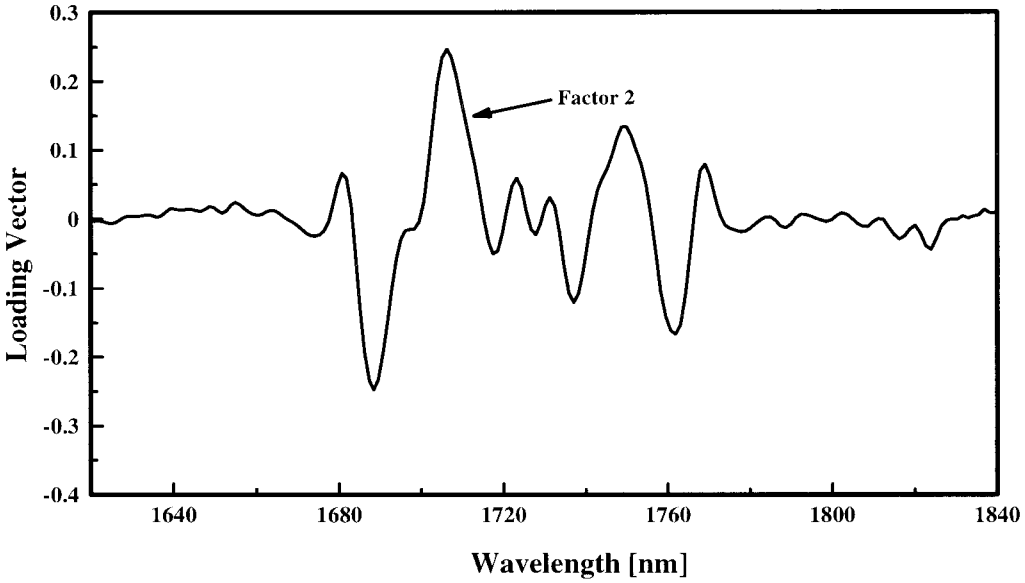

Figure 11 PLS calibration of $\mathbf{t}_{1,PCA}$: loadings plot for the second factor. The loading vector for the second principal component contains information about rheological response (secondary variation) in EVA copolymers. The loading weights are higher in the wavelength regions corresponding to shoulders of the C—H stretch peaks.

fore, the first factor has most of the information about VA content variation, but only some information about the rheological response.

The "secondary" effects on NIR spectra, due to rheological flow, are expected to dominate in the higher factors. As observed in Table II, the second principal component contains maximum information about the rheological response because this principal component explains maximum variance in **Y** data (an additional 63.4% variance is explained by the second factor). The loading and score vectors for the second principal component should explain this feature. Figure 11 shows a plot of the second loading vs. the NIR wavelength. It is observed that higher loading weights are associated with absorbances in the wavelength region of 1680–1720 nm. This region corresponds to the shoulder of the methylene stretch. (Note the presence of the shoulder in the overlaid absorbance plot in the earlier publication.)[1] Changes in the slope of the shoulder are observed about an inflection point at around 1715 nm, which lies in a trough in the first derivative plot. A similar observation is made in the wavelength regions of 1730–1745 nm and in 1745–1760 nm, which form shoulders of the doublet peaks.

By looking at the loadings in the first derivative domain, it is possible to determine which wavelengths have heavier loadings in the original absorbance spectrum. This observation is presented in a schematic form in Figure 12. For example, it is seen in Figure 12 that the wavelength region of 1700 to 1710 nm shows higher loading weights for the second principal component. Combining this information with that obtained from Table II, it is concluded that the variance in absorbance values in this wavelength region explains information pertaining to the rheological response. Similarly, other wavelength regions are identified that contain information about the $|\eta^*(\omega)|$ response. Based on the qualitative analysis using loadings plots, Figure 13 illustrates the wavelength regions in the original absorbance plot that are identified with information relating to VA content and rheological response.

Origin of Spectral Information Relating to Rheological Response

It is tempting to assume that these wavelength regions, which correlate with the rheological properties, contain information about end-group concentrations. It is common knowledge that polymer chain end-group concentrations are inversely proportional to average molecular weight, and moni-

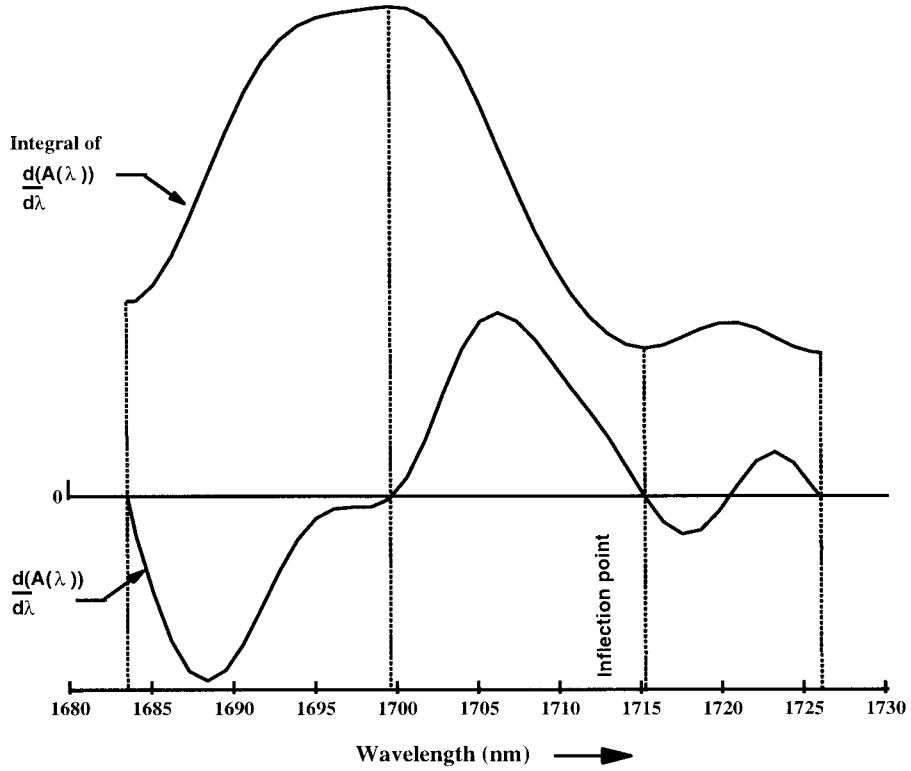

Figure 12 Schematic illustrating a methodology to identify the wavelength regions in the original absorbance spectrum with heavy loading weights for a given factor, for example factor 2 in Figure 11.

toring these concentrations has led to direct correlations with molecular weight parameters in earlier studies.[8] However, such work has been done only with polyol oligomers, or very low molecular weight macromolecules, especially with hydroxyl groups, which have strong spectral signatures in NIR. In the present study, for the high molecular weight EVA copolymers, a rough estimate of the typical end-group concentration, from the polymer number-averaged molecular weight and monomer molecular weights, gave a value of around 0.2%. Such concentrations are very low compared to the strong main chain signature due to C—H stretches. Hence, for the current system, it seems unlikely that the end-group measurements have any direct correlation with rheological properties.

One the other hand, during flow of molten EVA copolymers in a polymeric process such as extrusion, anisotropic flow effects on NIR spectra become significant. For the current experimental setup, the flow cross-section of these molten polymers changes from 9.5 × 2.5 mm at the exit port of the gear pump to a restricted cross-section of 2.5 × 2.5 mm in the optical measurement volume of the flow cell. Figure 14 shows a schematic of the contraction in flow that leads to orientation of the flowing polymer chains. Under constant nominal shear rates ($\sim 25\ s^{-1}$), these polymers would exhibit orientation effects that would vary with differences in molecular weight parameters. Subsequently, these factors would affect the NIR absorption spectra, though to a lower order magnitude compared to the strong variations due to chemical composition. It is assumed that these effects are also nonlinear; and hence, using natural logarithms of the material functions during regression, amounted to extracting a first-order relationship from the rheology-absorbance correlation.

Thus, this methodology was used to separate two features—varying VA content and varying rheological behavior—from the absorbance spectra. The score vector for the second factor was plotted against the response variable vector $\mathbf{t}_{1,PCA}$, as shown in Figure 15. If the rheological behavior were completely identified in the second factor alone, then the score vector for the second

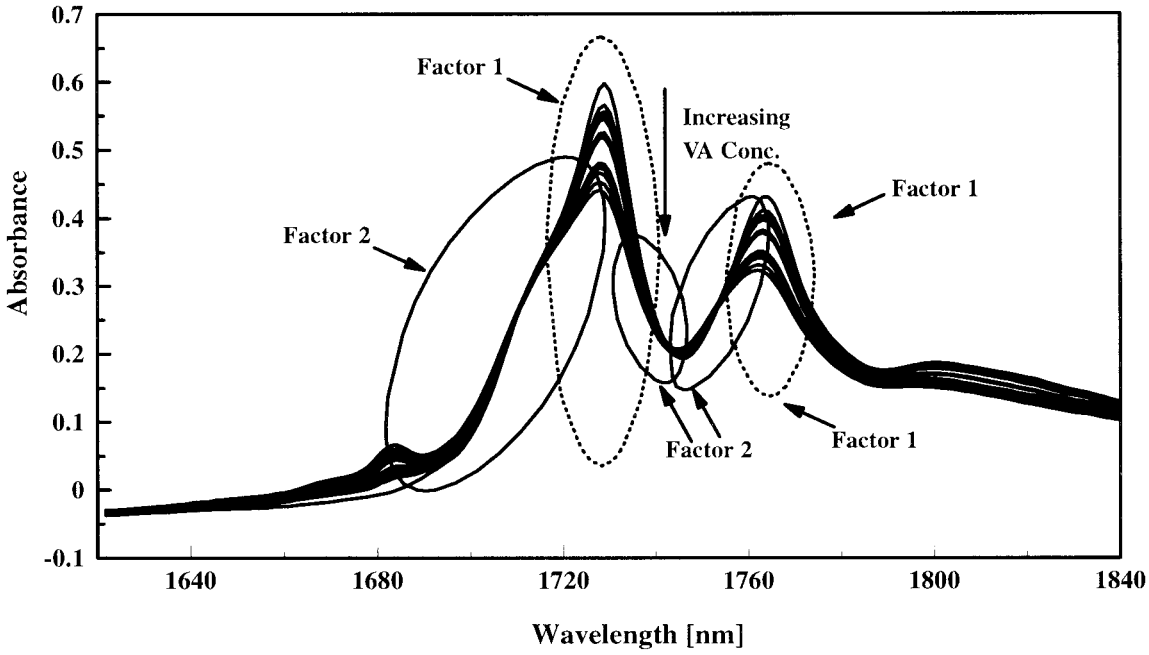

Figure 13 Overlaid plot of NIR absorbance spectra of EVA copolymers in the C—H stretch, first overtone region (1620–1840 nm). The wavelength regions associated with the primary variation, VA content (Factor 1); and the wavelength regions correlating with secondary variation, rheological properties (Factor 2) are identified from PLS analysis.

factor would be expected to show a strictly linear relationship with $\mathbf{t}_{1,\mathrm{PCA}}$. Because the second factor alone is not sufficient for predicting rheological response, only a general trend of linearity is observed in the second score plot of Figure 15. One reason for the deviation from linearity is the lack of samples available for calibration with uniform distribution of rheological properties. (Note the "holes" in calibration data in the higher end of calibration set, which is evident from the values of $\mathbf{t}_{1,\mathrm{PCA}}$ in Fig. 15.)

Real-time Predictions in an In-Line Extrusion Process

Finally, the stability of the predictions using the calibration model was tested in a real-time in-line extrusion process. Four Group I samples, followed by four Group II samples, which were not included in the calibration set, were continuously fed into the extruder, and test scans taken. Two samples with very low $|\eta^*(\omega)|$ values (MI = 143 g/10 min and MI = 370 g/10 min) were excluded from the analysis, as they gave larger residual errors. As explained in the previous section, these large errors are attributed to lack of a uniform distribution of sample space. Each absorbance scan was preprocessed and used for predictions of the rheological response. The calibration model built on the reduced response matrix, $\mathbf{t}_{1,\mathrm{PCA}}$, was used to predict the $\hat{\mathbf{t}}_{1,\mathrm{NIR}}$ value for each test scan. Therefore, for every test scan, a value for $\hat{\mathbf{t}}_{1,\mathrm{NIR}}$ is predicted. The $\hat{\mathbf{t}}_{1,\mathrm{NIR}}$ values are plotted against the extruder run time in Figure 16. The detection limits for predictions are decided by the SEP values obtained from the calibration model. It is observed that most predictions lie within the limits defined by the SEP.

Once the predicted $\hat{\mathbf{t}}_{1,\mathrm{NIR}}$ values are obtained by PLS, the entire complex viscosity response is regenerated using eq. (7), as explained in the previous section. Therefore, for every test scan, one linear viscoelastic curve was estimated. Several such curves, which were obtained over the entire extruder run time, are shown in Figure 17 as a thre-dimensional plot. This plot shows the complex viscosity response vs. ω with polymer extrusion time. As observed during the predictions of MI in near real time, the transition of $|\eta^*(\omega)|$ response is smooth from one sample to another.

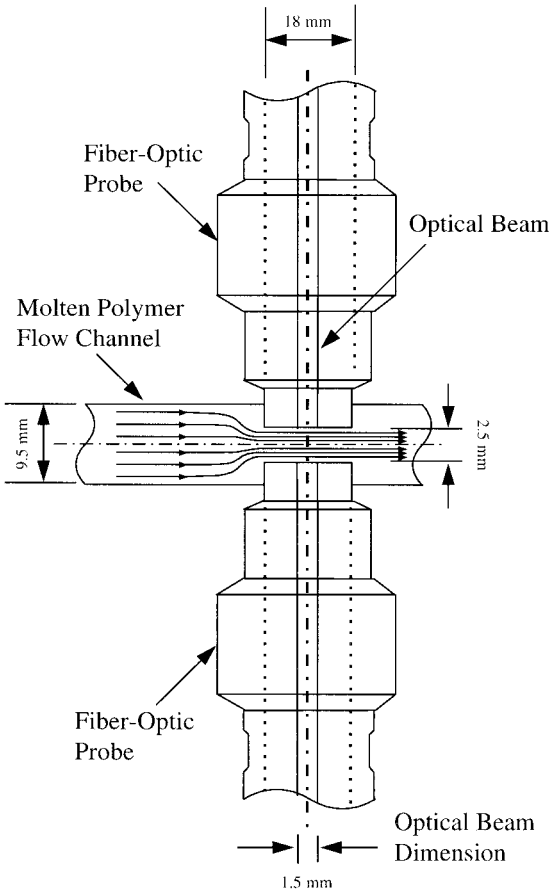

Figure 14 Schematic representation of contraction flow through the flow cell.

The transition region also indicates the average residence time of the sample in the polymer monitoring system.

EXPERIMENTAL LIMITATIONS

In the experimental set of EVA samples chosen, the rheological data showed only one factor of variation. This conclusion is drawn from the results obtained from PCA analysis, which showed that the first principal component captured about 99.82% variation. This meant variation in only one physical factor, probably differences in polymer average molecular weight among various EVA samples. (The polymerization process and termination conditions were similar for these random copolymers from both manufacturers.) Such variation in molecular weight values resulted in a vertical shift in various complex viscosity responses. With additional physical parameters, such as branching parameters and MWD affecting rheological behavior, the resulting rheology data will be more complex. In such cases, PCA analysis will highlight the need for larger number of principal components to explain significant variance in the **Y** data. However, this experimental limitation does not imply a deficiency in the calibration methodology. With additional factors required for PCA, the procedure for PLS regression will remain essentially same. Only, additional calibration models need to be developed for predictions of several principal components, $\mathbf{t}_{\mathbf{j,PCA}}$, $\{j = 1, \ldots, k\}$. The entire rheological response can still be regenerated from eq. (7). Because these additional physical parameters are also expected to affect the rheological flow behavior during extrusion, and subsequently, the NIR absorption spectra, the methodology described in the previous sections should hold for complicated rheological behavior as well.

Temperature is an important variable, which would have a large effect on rheological properties, but only a subtle peak-shifting effect in the NIR data. The current study has focused only on isothermal studies, and temperature was not included as an independent variable during calibration. During extrusion, factors such as viscous heating will lead to significant temperature changes; although for this study, a precise quantitative measurement was not available for estimating such temperature increase. However, the operating conditions for the linear viscoelastic experiments, and for extrusion, were held within nominal fluctuations about the temperature set point. Also, it should be noted that the strong effect of temperature on rheological properties is suppressed to a great extent by using natural logarithms of the rheological functions during calibration. Another strategy to include temperature variations is to perform the linear viscoelastic experiments on each of these EVA copolymers at different temperatures. The temperature range for these measurements should be chosen to include the maximum expected increase from viscous heating. A strategy involving PCA can be developed, similar to the one developed earlier, where the linear viscoelastic response curves at varying temperatures for each EVA sample is superposed onto a single master curve (or first loading vector). Subsequently, these master curves for the EVA samples can be used to develop the calibration model, using the methodology described in this article. Given an EVA sam-

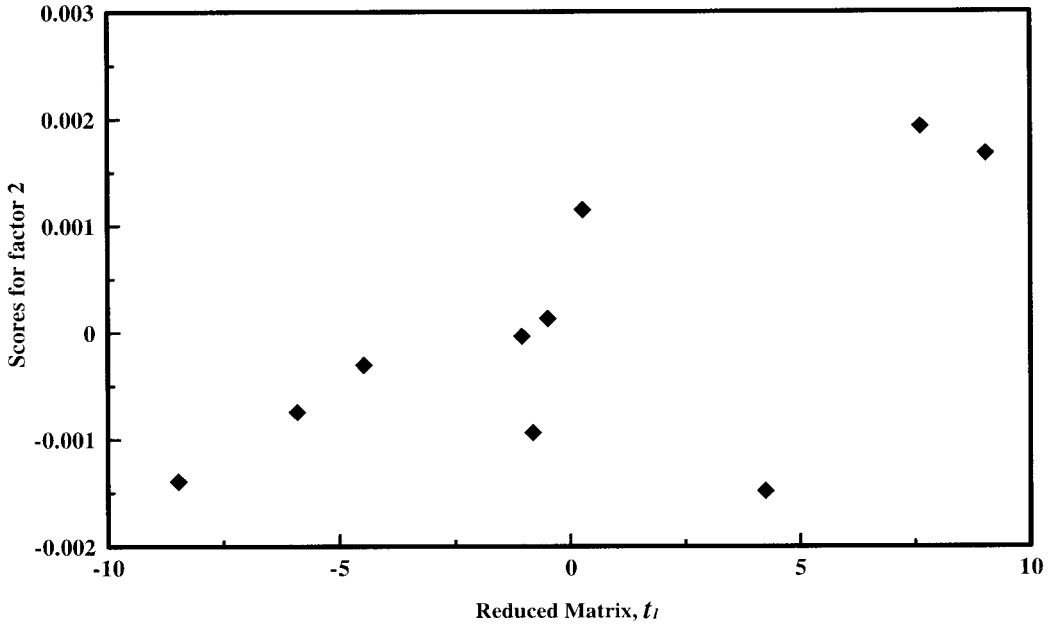

Figure 15 PLS calibration of $\mathbf{t}_{1,PCA}$: scores plot for the second factor. If the second factor had complete information about the rheological response, a strictly linear trend would be expected. Because additional factors are required, only a general trend in linearity is observed. Also, this score vector reflects the lack of uniform distribution of sample properties for the calibration model.

ple with unknown complex viscosity response, the calibration model can be used to estimate its master curve; and the actual response at the measured temperature can be regenerated using the corresponding shift factor (or first score vector).

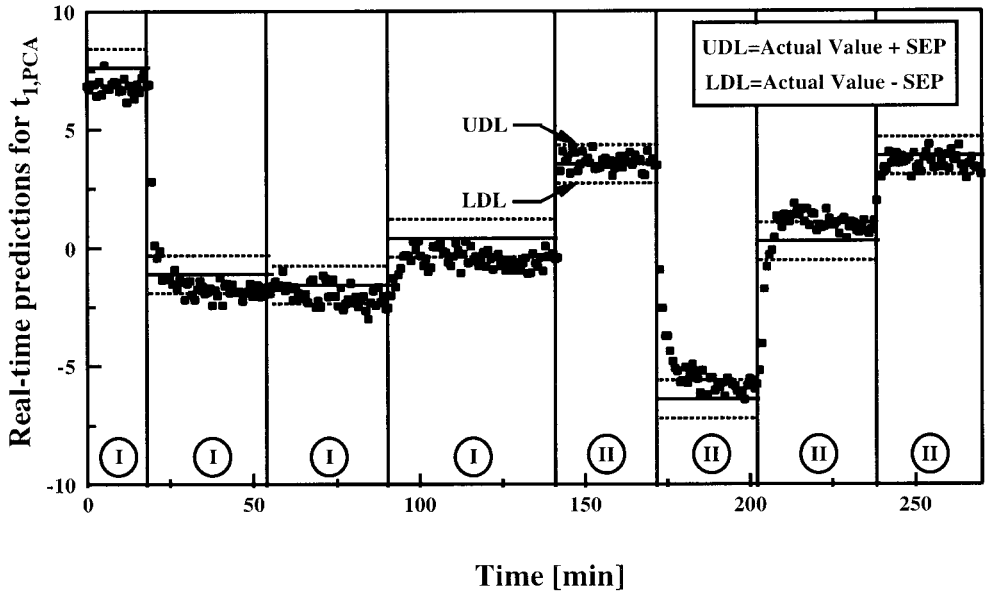

Figure 16 In-line real-time predictions of $\hat{\mathbf{t}}_{1,NIR}$ in Group I and Group II samples: Four Group I samples followed by four Group II samples were fed into the extruder in an extrusion process and test scans collected: the predictions lie within the SEP limits associated with the calibration models. (SEP = 0.80; UDL = upper detection limit; LDL = lower detection limit.)

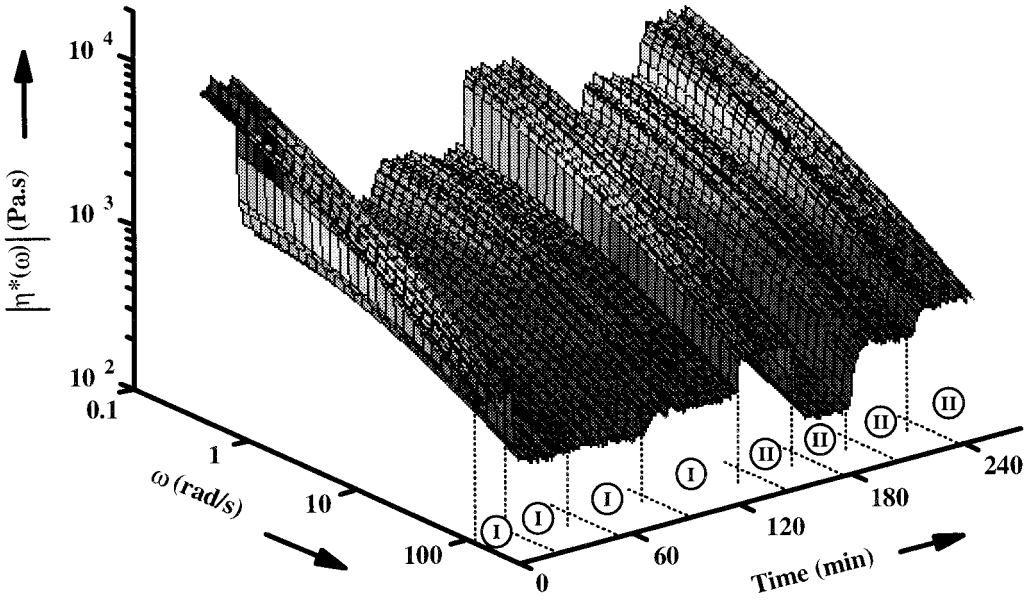

Figure 17 Three-dimensional plot showing the real-time predictions for the rheological response of Group I and Group II samples (these samples were not included during calibration): the complex viscosity curves are regenerated from the PLS-predicted $\hat{\mathbf{t}}_{1,\mathrm{NIR}}$ values (shown in Fig. 16) using eq. (7). The rheological data used for correlation with NIR spectra had only physical factor of variation.

The calibration model built here is by no means universal in its applicability to all EVA polymers using any near-infrared instrument. However, a methodology has been proposed, and feasibility of its use has been successfully demonstrated for estimating complex viscosity responses with one factor of variation. Typically, a very large set of samples is required to build a robust calibration model. It is crucial for such a large sample set to include samples with uniform and wide variation in the rheological parameters. Also, the distribution of the $\bar{M}_w$ parameters and VA content in these samples should be random. At the same time, it is important that the entire ranges of VA and rheological variations (the primary and secondary factors of variation, respectively) be represented in the calibration set.

CONCLUSIONS

The "primary" or the dominant factor of variation in the NIR absorption spectra is the VA content in the copolymer, and appears as the first principal component. The "secondary" factors that affect the absorption spectra are attributed to the anisotropic rheological flow behavior of molten polymers during extrusion. Under nominal shear rates, the level of molecular orientation will be different for flowing polymer melts associated with varying molecular weight parameters. This anisotropic nature of flow will result in lower order magnitude effects on absorption spectra. These subtle variations in NIR spectra appear in higher factors or loadings; and correlate with polymer rheological properties, such as linear viscoelastic material functions.

In conjunction with predictions of MI,[1] it has been shown for molten EVA copolymers, that dynamic linear viscoelastic properties, which have one factor of variation, can be estimated using in-line fiber-optic NIR spectroscopy. The calibration models are robust in that predictions are stable in a real-time process, and lie within SEP limits set by the models. Temperature effects on the spectra are also significant, though in this study, the temperatures of the molten polymer in the flow cell remained constant with a minimal variance of about 1–3°C. However, the calibration models can be further improved by including temperature as an independent variable alongside the absorbance spectra, in the **X** matrix. The methodology presented here

for $|\eta^*(\omega)|$ would be equally applicable to $\eta(\dot{\gamma})$ vs. $\dot{\gamma}$, the shear rate data.

NOMENCLATURE

Symbol Abbreviation	Description
α	Matrix of regression coefficients, obtained from PLS regression
β	Regression coefficient vectors, obtained from PLS regression
$\|\eta^*(\omega)\|$	Complex viscosity, expressed as a function of ω (Pa·s)
Σ	Diagonal matrix with singular values as diagonal elements
ω	Angular frequency (rad/s)
B	Matrix of regression coefficients, obtained from PLS regression
EVA	Ethylene–vinyl acetate copolymer
$G'(\omega)$	Storage modulus, expressed as a function of ω(Pa)
$G''(\omega)$	Loss modulus, expressed as a function of ω(Pa)
j	Array
k	Array
LAS	Leave-a-sample crossvalidation approach
LDL	Lower detection limit for quantification
MI	Melt flow index (g/10 min)
$\bar{M}_w$	Weight average molecular weight of the polymer (g/mol)
MWD	Molecular weight distribution in the polymer
m	Index, number of rows in a matrix
NIR	1. Near-infrared 2. Used as a subscript to denote results from regression with NIR data
n	Index, number of columns in a matrix
PCA	1. Principal component analysis 2. Used as a subscript to denote results from PCA analysis
PLS	Partial least squares
PRESS	Predicted residual sum of squares
reg	Used as a subscript to denote a regenerated matrix, after PCA analysis
SEC	Standard error of calibration
SEP	Standard error of prediction
SVD	Singular value decomposition of a matrix
T	Scores matrix
T	Used as a superscript to denote transpose of a matrix
t	Score vector, column of matrix **T**
U	Scores matrix or left eigenvector, obtained from SVD analysis
UDL	Upper detection limit for quantification
V	Right singular vector, obtained from SVD
VA	Vinyl acetate comonomer, in EVA copolymer
X	NIR absorbance data matrix
Y	Rheology data matrix
y	Vector, column of Y
$\hat{}$	Symbol used to denote estimated values of variables, obtained from regression

REFERENCES

1. M. G. Hansen and S. Vedula, *J. Appl. Polym. Sci.,* to appear.
2. A. Hoskuldsson, *J. Chemometr.,* **9,** 91 (1995).
3. A. Hoskuldsson, *J. Chemometr.,* **9,** 91 (1995).
4. H. Martens and T. Naes, in *Multivariate Calibration,* John Wiley & Sons Ltd., New York, 1989.
5. J. Sun, *J. Chemometr.,* **10,** 1 (1996).
6. J. D. Ferry, in *Viscoelastic Properties of Polymers,* John Wiley & Sons, Inc., New York, 1980.
7. R. B. Bird, R. C. Armstrong, and O. Hasseger, *Dynamics of Polymeric Liquids,* John Wiley & Sons, Inc., New York, 1987.
8. D. A. Burns and E. W. Ciurczak, in *Handbook of Near-Infrared Analysis,* Marcel-Dekker, Inc., New York, 1992.